The International Journal of Advanced Manufacturing Technology (2022) 119:3533–3544
https://doi.org/10.1007/s00170-021-08630-x

ORIGINAL ARTICLE

Study on the cutting characteristics of high-speed machining Zr-based bulk metallic glass

Haidong Yang[1] · Yusong Wu[1] · Junsheng Zhang[1] · Huohong Tang[1] · Weijie Chang[1] · Juchen Zhang[1] · Shunhua Chen[1]

Received: 10 August 2021 / Accepted: 21 December 2021 / Published online: 7 January 2022

Abstract

The cutting characteristics of high-speed machining (100–350 m/min) $Zr_{57}Cu_{20}Al_{10}Ni_8Ti_5$ (at.%) bulk metallic glass (Zr57 BMG) were studied, as compared with industrial pure zirconium (Zr702). The effect of cutting speed on cutting force, surface roughness, surface morphology, chip morphology, and tool wear was analyzed. Although the strength of Zr57 BMG is much higher than that of Zr702, there is no significant difference between the main cutting forces of the two materials, which can be attributed to the thermal softening of Zr57 BMG material during machining. The machined surface characteristics and the formation of chips were investigated. Differing from low-speed machining, the groove marks and adhensions on machined surface evolve to wave patterns and molten droplets when the cutting speed increased from 100 to 350 m/min. The appearance of wave patterns tends to destroy the machined surfaces, and the worst quality was obtained at the speed of 250 m/min. The free surface morphology of the chips, with cutting speed smaller than 150 m/min, show obvious serration and molten droplets between the shear bands. With the increase of cutting speed, oxidation on the chip surfaces occurred, and the chip surface was gradually covered by powder particles due to the melting of Zr57 BMG workpiece materials. The wear behavior of the flank faces of cutting tools was also examined. After high-speed machining, the machined surfaces of the Zr57 BMG still maintain the amorphous atomic structures. The cutting parameters at relatively high cutting speed (from 250 to 350 m/min) were further optimized for improving the machined surface quality. The present findings are of significance for the processing of BMG and BMG components by use of high-speed machining.

Keywords Metallic glass · Cutting speed · Cutting force · Surface roughness · Chip morphology

1 Introduction

Significantly different from traditional alloys, bulk metallic glasses (BMGs) are a new kind of metallic materials, which have unique mechanical and physical properties and wide range of application prospects [1]. Machining has been used extensively for the processing of metals and alloys in industry, where the cutting performance and mechanisms were also studied for the structural applications of new classes of alloys [2, 3]. The machining of BMGs therefore attracted a great deal of research attention [4–6]. For example, Bakkal et al. studied the cutting performance of Zr-based BMG by turning, drilling, milling, and grinding [7–10]. The results showed that excellent dimensional accuracy and surface quality can be obtained with conventional machining processes. Fujita et al. [11] also found that BMGs have excellent machinability due to the absence of built-up edges (BUE) during machining. Bakkal et al. [12] found that the chip crystallization behavior was intensified with the increasing of cutting speed, where light emission was observed during machining. However, differing from the crystallization of chips, no crystallization occurred on the machined surface of BMG at different cutting speeds, implying the feasibility of the machining of BMGs. The effect of cutting temperature on the generation and propagation of shear band was then studied [13]. The results showed that the thermal instability of shear band was the main reason for the plastic deformation behavior of BMG, which exhibited excellent plastic deformation performance during machining.

However, due to the necessities to achieve rapid cooling rate to form glassy atomic structures, BMGs are known to

✉ Junsheng Zhang
zhangjunsheng90@126.com

✉ Shunhua Chen
shchen@hfut.edu.cn

[1] School of Mechanical Engineering, Hefei University of Technology, Hefei 230009, China

have limited sample dimensions, and the studies of BMG machining mainly focused on low-speed and micro machining. For example, Gong et al. [14] conducted the micro grinding of Zr-based BMGs. The results showed that the material removal mode of the Zr-based BMG was plastic with CBN abrasive micro grinding wheel, and the material removal mode was brittle with the diamond abrasive micro grinding wheel. At the same time, the grinding temperature was simulated and the maximum value was 288 °C within the range of experimental parameters. Chen et al. [15] studied the cutting performance of a $Zr_{55}Cu_{30}Al_{10}Ni_5$ (at.%) BMG during ultra-precision machining, and found that BMG showed excellent plasticity during the cutting process. The best surface roughness can reach 100 nm, and a mirror surface cannot be obtained because of the viscous flow during machining. Zhu et al. [16] studied the nano cutting process of a $Cu_{50}Zr_{50}$ (at.%) BMG using molecular dynamics (MD) simulations, and found that the material removal mechanism was mainly based on nanoscale extrusion rather than macroscale shear deformation.

Previous studies on the micro turning of BMG also revealed that the variation of cutting speed had little effect on cutting force at low liner velocity [17]. At the speed of 1.52 m/s, the extremely high temperature during machining will induce the oxidation of chips accompanied with light emission. On the contrary, no chip oxidation and light emission occurred when the cutting speed decreased to 0.38 m/s [18]. Because of the low thermal conductivity of BMG [19], the generated cutting heat was difficult to be transferred, which would lead to a temperature rise in the cutting zone. Besides, serrated chips are typical features during the cutting of BMG. Jiang et al. [20] demonstrated that the formation of serrated chips was mainly due to the repeated formation of shear bands in the primary shear zones (PSZs). Maroju et al. [21] found that the inhomogeneous deformation of BMG chips was mainly influenced by the cutting temperature and free volume. Additionally, Dhale et al. [22] found that with the increase of cutting speed, cracks will form in individual serrated regions due to the propagation of shear bands.

In recent years, although many studies were carried out on the machining of BMGs, and fruitful achievements were made, the studies on the cutting performance of BMGs at speed larger than 150 m/min have rarely been reported under regular cutting condition due to the sample-size limitation. A higher cutting speed will produce a higher cutting temperature during machining, which will have a significant impact on the cutting force, machined surface morphology, chip morphology, surface quality, and tool wear. The deformation characteristics and amorphous atomic structures of BMGs at high-speed machining should also be different from the results at low-speed machining. In this work, high-speed turning of a Zr-based BMG was conducted, with cutting speed ranging from 100 to 350 m/min. The cutting force, surface morphology, chip deformation, and tool wear during the high-speed machining of BMG were examined and analyzed, giving more insight into the high-speed machining performance of BMGs.

2 Methodology

$Zr_{57}Cu_{20}Al_{10}Ni_8Ti_5$ (at.%) BMG (noted as Zr57 BMG) was used as the workpiece material for high-speed machining. The as-cast BMG rods with sizes of 90 mm × Φ5 mm were produced by suction casting. Industrial pure Zr (Zr702) rods with same sample dimensions were used for comparison. The mechanical and physical properties of the two workpiece materials are presented in Table 1.

The turning process was carried out on a CA6140 lathe with a maximum spindle speed of 1440 r/min. The lathe was equipped with a three-dimensional dynamometer Kistler 9257B and a frequency converter (3G3RV-A4075-ZV). The axial force *Fx*, radial force *Fy*, and main force *Fz* were recorded by the dynamometer. The dynamometer has a relatively high resolution and good reliability, and the sensitivity of *Fx*, *Fy*, and *Fz* are 7.5 *pC/N*, 7.5 *pC/N*, and 3.7 *pC/N*, respectively. The measuring ranges of *Fx*, *Fy*, and *Fz* are 5 *kN*, 5 *kN*, and 10 *kN*, respectively, and the threshold is smaller than 0.01 N. In order to achieve the high-speed machining of BMGs with limited sample diameters, a special fixture device was designed, as shown in Fig. 1. The fixture was a 45-steel bar with a diameter of 90 mm. Three arc slots of 5 mm diameters were machined at the end surface of the bar. A cover plate and several bolts were then used to fix the workpiece material rods in the arc slots along the axis direction. High-speed machining of BMG was realized by means of intermittent turning, and the maximum cutting speed can reach 350 m/min, which was much higher than the reported data in literature (about 150 m/min) [11]. The experimental setup, including the setting of the cutting tool and the use of fixture device, is shown in Fig. 1.

Table 1 Mechanical properties of two kinds of workpiece materials

Materials	Yield strength (MPa)	Elastic modulus (GPa)	Thermal conductivity (W/m · K)	Hardness ($HV_{0.5}$)	Melting point (°C)
Zr57 BMG	1635	82.0	7.1	537.7	822
Zr702	205	99	22	189.9	1852

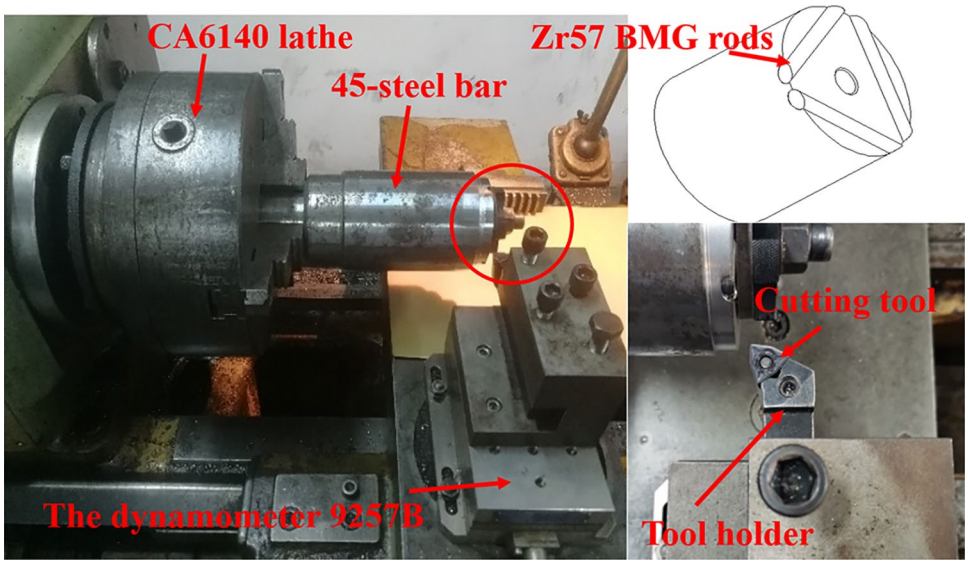

Fig. 1 The experimental setup as well as the schematic diagram showing the fixture device for high-speed machining

During the intermittent turning of BMGs, the actual cutting distance of BMG specimen was short and the corresponding machining time was also short. In order to better measure the cutting force, the sampling frequency of the dynamometer was set as 5000 Hz.

During the cutting process, the cutting parameters used in this research were 100 to 350 m/min for cutting speed v, 0.2 mm for cutting depth a_p, and 0.08 mm/r for feed rate f, respectively. Cemented carbide inserts (YBG302 with TiAlN coated) were used for the high-speed machining, and the cutting condition was dry cutting. The geometric parameters of the cemented carbide inserts are given in Table 2. The surface roughness of the machined surface was examined with the JH-340 roughness measuring device. The surface and chip morphologies were inspected using scanning electron microscopy (SEM) and energy dispersive spectrometer (EDS) on an SU8020 field emission scanning electron microscope. The machined surfaces were inspected using standard X-ray diffraction (XRD) analysis to study the possible change of amorphous atomic structures.

3 Results and discussion

3.1 Cutting force

The cutting forces for the machining of Zr57 BMG and Zr702 are shown in Fig. 2. It shows that the cutting forces of *Fx*, *Fy*, and *Fz* increase with the cutting speed ranging from 100 to 350 m/min. For the machining of Zr57 BMG, the radial force *Fy* was larger than *Fx* and *Fz*. Significantly different from the machining of Zr57 BMG, the main cutting force *Fz* was the largest one for Zr702. The extremely high yield strength and hardness of Zr57 BMG could be the main reason for the high radial force. Moreover, the absence of corner radius of 0.8 mm obviously reduced the actual major cutting edge angle, which would also result in the increase of radial force *Fy*. However, there is no significant difference between the main cutting forces (*Fz*) of the Zr57 BMG and Zr702 workpiece materials. The cutting temperature of Zr57 BMG would be high because of its low thermal conductivity. It can then cause the thermal softening effect during machining and result in the decrease of main cutting force *Fz*. In general, the axial force *Fx* and radial force *Fy* of Zr57 BMG were both larger than those of Zr702. It mainly depends on the high yield strength and hardness of the Zr57 BMG material. While for the main cutting force *Fz*, it mainly depends on the stress in the chip shear deformation zone, where the cutting heat is concentrated. With the thermal softening effect, the stress in the chip shear deformation zone of Zr57 BMG was significantly reduced, resulting in smaller *Fz* values comparable the results of Zr702 with much lower strength and hardness.

3.2 Surface roughness and morphology

The machined surface roughness of Zr57 BMG and Zr702 data are presented in Fig. 3. With the cutting speed ranging from 100 to 350 m/min, the surface roughness of Zr702 decreased gradually from 3.6 to 1.5 μm. For Zr57 BMG,

Table 2 Geometric parameters of the cemented carbide inserts

Rake angle γ_o	Clearance angle α_o	Major cutting edge angle κ_r	Inclination angle λ_s	Corner radius r_ε	Coating
0°	0°	91°	0°	0.8 mm	TiAlN

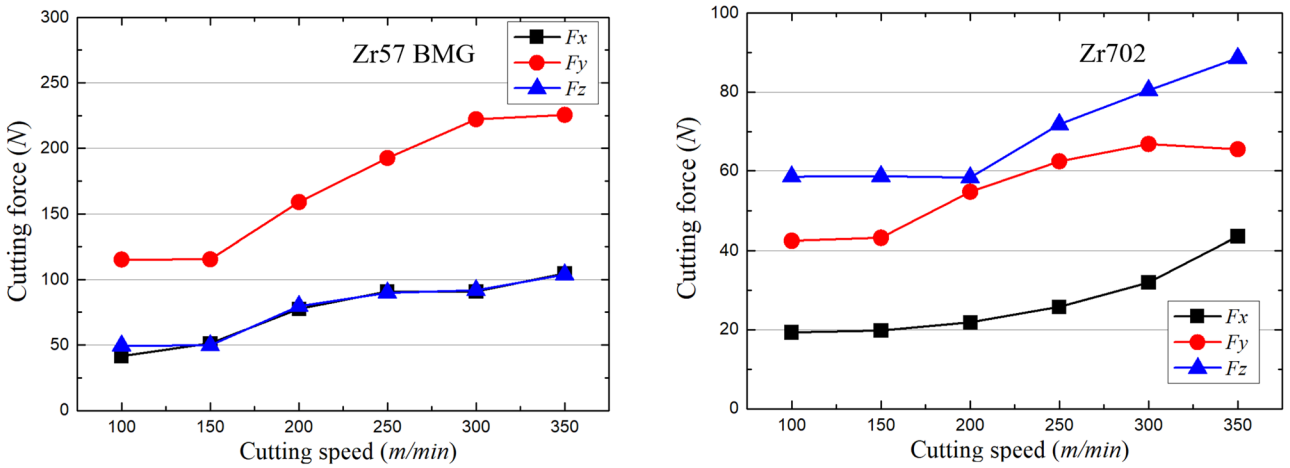

Fig. 2 The cutting forces for the machining of Zr57 BMG and Zr702

the surface roughness first increased and then decreased, and reached the highest value of 2.4 μm at the speed of 250 m/min. The surface quality of Zr57 BMG was better than that of Zr702 when the cutting speed was smaller than 250 m/min. When the speed was larger than 250 m/min, the difference of surface roughness between Zr57 BMG and Zr702 was small.

In order to further study the variation trend of the surface roughness of Zr57 BMG, the machined surface morphology is presented in Fig. 4. Generally, the surface morphology can reflect the characteristics of the material deformation process [23]. Groove marks along the cutting direction of the insert and adhensions were observed on the machined surface when the cutting speed was smaller than 150 m/min (Fig. 4a, b). Here, the appearance of groove marks was mainly due to the combination effect of extrusion stress on tool-workpiece interface and cutting temperature, which would cause the plastic deformation of the workpiece material. The adhensions on the machined surface were mainly caused by the debris of the workpiece material during machining. It indicates that the machined surface of Zr57 BMG shows certain plasticity and viscosity, and finally generates groove marks and adhensions when the speed is smaller than 150 m/min.

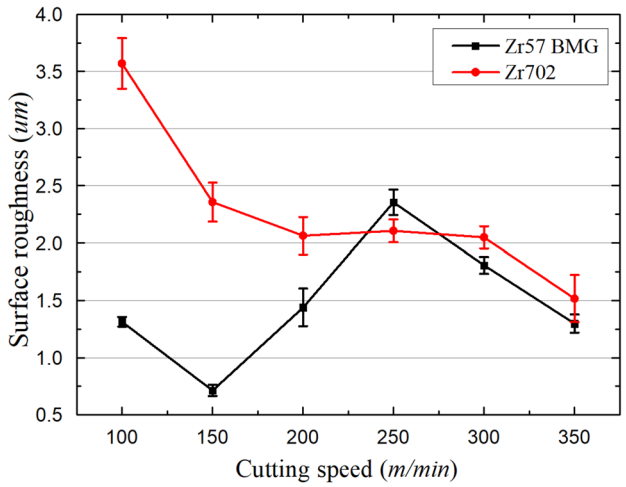

Fig. 3 Surface roughness of Zr57 BMG and Zr702 at different cutting speeds

When the cutting speed increased to 200 m/min (Fig. 4c), the groove marks and adhensions on machined surface began to disappear gradually, which were replaced by wave patterns and molten droplets. Here, the cutting temperature increased with the increase of speed. When the temperature on the machined surface increased to the glass-transition temperature (T_g), the BMG material will undergo thermal softening, showing excellent liquidity and poor viscosity. The excellent liquidity and poor viscosity could be the main reason for the disappearance of groove marks and adhensions, and the appearance of wave patterns and molten droplets. When the cutting speed was larger than 200 m/min, the wave patterns and molten droplets were more obvious at relatively higher speeds, as shown in Fig. 5. The wave patterns were formed due to the liquid flow of melted workpiece material under the combined action of extrusion stress and temperature. At the speed of 250 m/min (Fig. 5a), the flow of wave patterns was irregular, which may be due to that the cutting temperature and liquidity of melted material were not high enough. When the cutting speed increased to 300 m/min (Fig. 5b) and 350 m/min (Fig. 5c), the flow of wave patterns became more and more regular. This could be attributed to the liquidity increases of the Zr57 BMG material with the increase of cutting temperature. It was also found that the molten droplets were always concentrated near the wave patterns. The scale of molten droplets increased with the increase of cutting speed, and it could evolve to wave patterns when the local temperature and stress were high enough. When the cutting speed increased to 350 m/

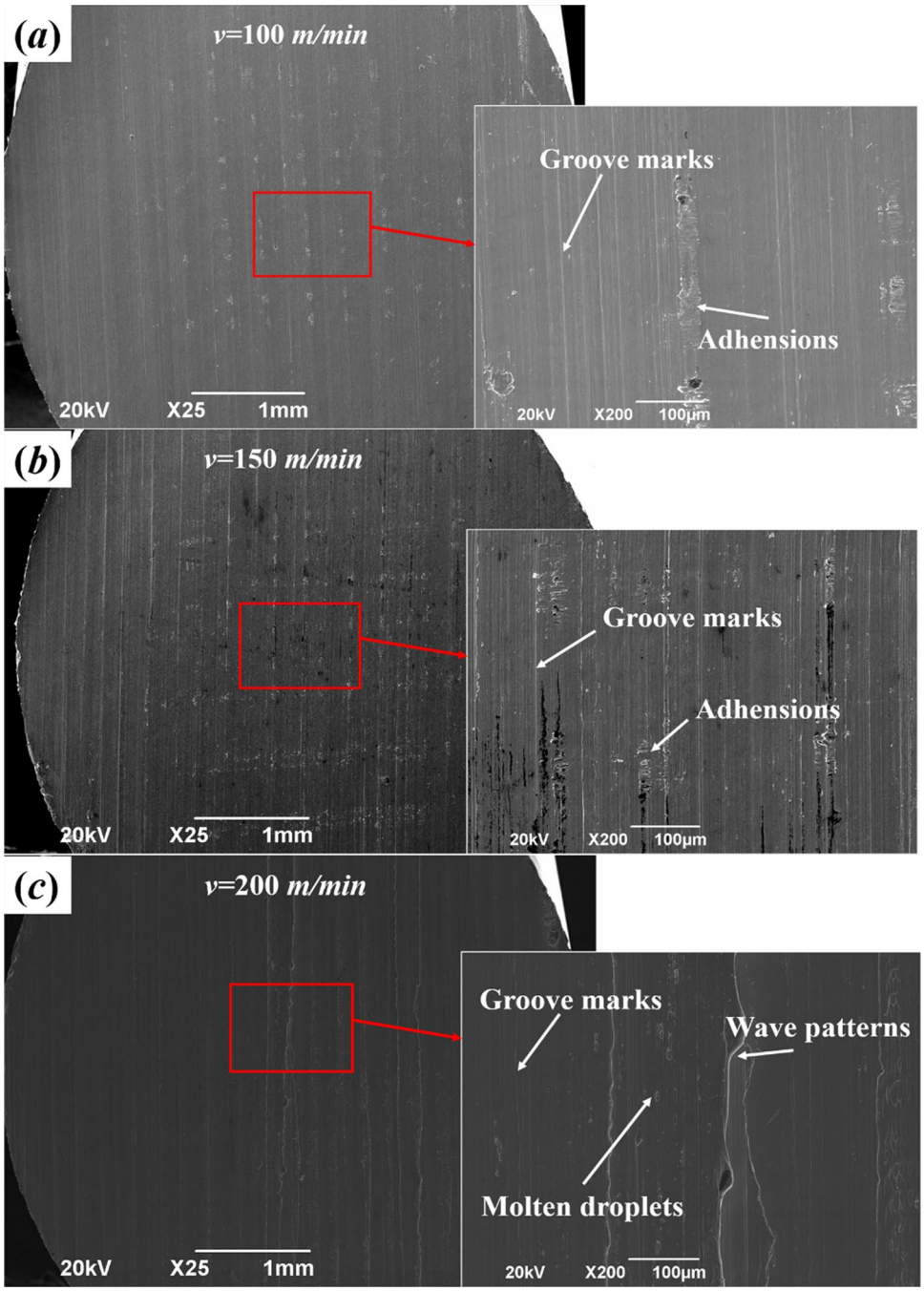

Fig. 4 Machined surface morphology of Zr57 BMG at the speed of 100 m/min (**a**), 150 m/min (**b**), and 200 m/min (**c**), respectively

min, the number of molten droplets decreased, but the sizes increased. The machined surfaces of Zr702 at the cutting speeds of 100 and 350 m/min were also shown in Fig. 6. Similar to Zr57 BMG, groove marks and adhensions were found on machined surfaces at relatively low cutting speed. However, when the speed increased to 350 m/min, differing from that of Zr57 BMG, the adhensions began to disappear, but groove marks were still observed. No wave patterns and molten droplets occurred on the machined surfaces, as shown in Fig. 6b. This phenomenon may result from the high thermal conductivity and melting point of Zr702 material.

For Zr57 BMG, temperature plays an important role for the forming of machined surface morphology. With the increase of cutting speed, the surface morphology showed certain plasticity and viscosity firstly, and then showed excellent liquidity and poor viscosity. The morphology of groove marks and adhensions also evolved to wave patterns and molten droplets. The surface roughness reached the highest value of 2.4 μm at the speed of 250 m/min (Fig. 5a), at which irregular wave patterns started to form. By comparing the surface roughness results and the morphology of machined surfaces, it can be found that the

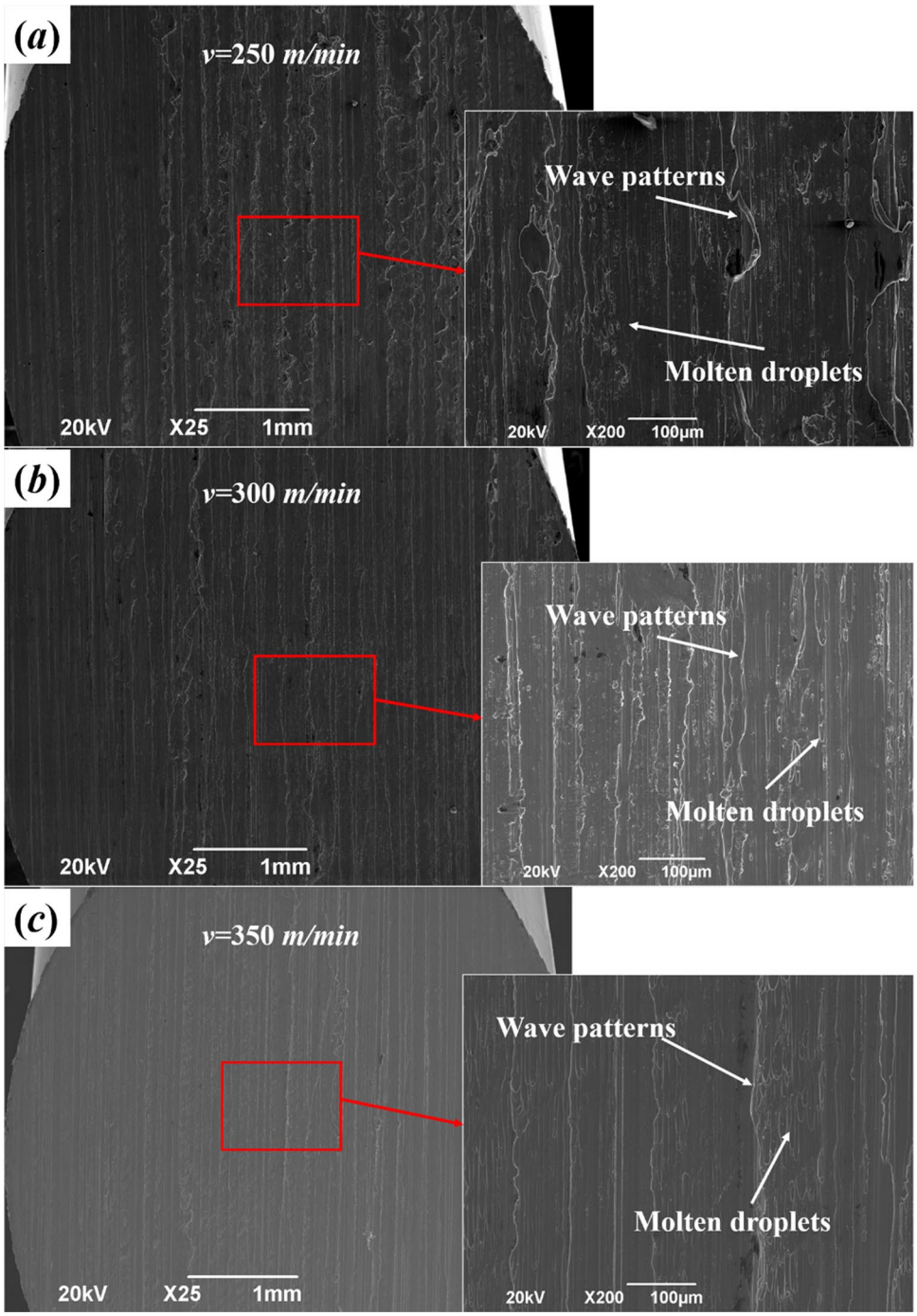

Fig. 5 Machined surface morphology of Zr57 BMG at the speed of 250 m/min (**a**), 300 m/min (**b**), and 350 m/min (**c**), respectively

wave patterns affected the surface roughness. The results showed that the appearance of wave patterns was more likely to destroy the surface quality, and the surface roughness reached the poorest value when the wave patterns distribution was irregular at the cutting speed of 250 m/min. With the cutting speed increasing to 350 m/min, the distribution of wave patterns became regular, and the surface quality was also improved. Differing from Zr57 BMG, the surface roughness of Zr702 decreased with the increase of cutting speed. In terms of machined surface morphology, the adhensions began to disappear at the speed of 350 m/min. Therefore, the decrease of adhensions can improve the surface quality. For Zr57 BMG, the appearance of wave patterns was mainly due to its low melting point, which can rarely be observed in Zr702 even at the cutting speed of 350 m/min. In general, the variation of surface quality can be explained by the evolution of machined surfaces morphology, which was mainly dependent on the

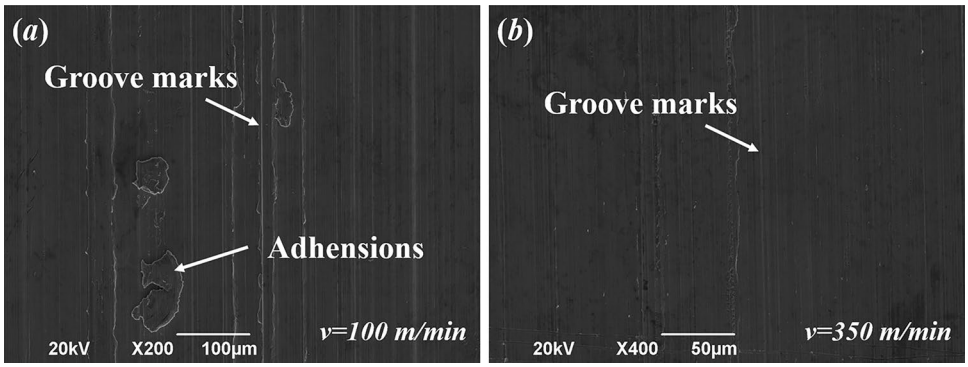

Fig. 6 Machined surface morphology of Zr702 at the speed of 100 m/min (**a**) and 350 m/min (**b**), respectively

material properties, such as melting point, plasticity, viscosity and liquidity.

Amorphous atomic structures make Zr57 BMG have excellent mechanical performance, while crystallization will destroy the amorphous structures and affect the material mechanical performance. During the high-speed machining of Zr57 BMG, the extremely high temperature may cause the crystallization of material. In order to confirm whether crystallization occurs on the machined surfaces, the microstructure of Zr57 BMG at different cutting speeds was characterized using standard X-ray diffraction (XRD) analysis and compared with as-cast Zr57 BMG specimen, as shown in Fig. 7. A diffuse reflection peak was observed for both the as-cast and machined surfaces of Zr57 BMG at different cutting speeds. And no sharp crystalline peak for crystals was observed. It indicates that although wave patterns and molten droplets were observed on the machined surfaces, there was no crystallization during the high-speed (100 m/min-350 m/min) machining of Zr57 BMG. Thus, despite with the generation of a large amount of heat during high-speed cutting, Zr57 BMGs can still maintain the amorphous atomic structures on machined surfaces, which shows excellent application potential for the processing of BMGs and BMG components.

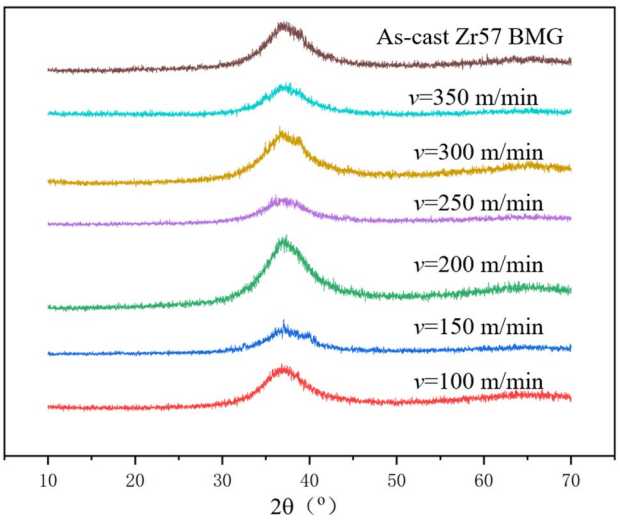

Fig. 7 XRD patterns of the machined surfaces of Zr57 BMG at different cutting speeds

3.3 Chip morphology

During machining, the formation of chips also affects the stability of cutting process. In order to study the chip morphology of Zr57 BMG at high-speed machining, SEM micrographs of chips were analyzed detailly, as shown in Fig. 8a–e. Due to the low thermal conductivity of Zr57 BMG, light emission was likely to occur during machining. Similar to the chip morphology of low-speed machining Zr57 BMG, the chip morphology of free surface with cutting speed smaller than 150 m/min showed obvious serration, as presented in Fig. 8a, b. And molten droplets between shear bands were observed, which were formed by the melting of workpiece material during the shear deformation process of chips. The appearance of molten droplets indicated that the temperature between two shear bands was close to the melting point of Zr57 BMG material during machining. Differing from high-speed machining, the molten droplets were not observed during the low-speed machining (4.2 m/min) of BMGs [20]. Besides, the primary shear zones and secondary shear bands were obvious during low-speed machining. The primary shear zones were formed with the shear slip, which will cause the stress degradation on the shear deformation zone, resulting in the formation of secondary shear bands. During high-speed machining, the cutting temperature was close to the melting point of the BMG material and melting occurred during the formation of chips. With the cutting speed increasing from 250 to 350 m/min (Fig. 8c–e), powder particles began to appear on the surfaces of serrated chips, and finally covered the chips completely. The chips still maintained the serrated shapes when the speed increased to 250 m/min. However, when the cutting speed increased to 300 and 350 m/min, the shapes of the chips became irregular, and the chips were completely covered

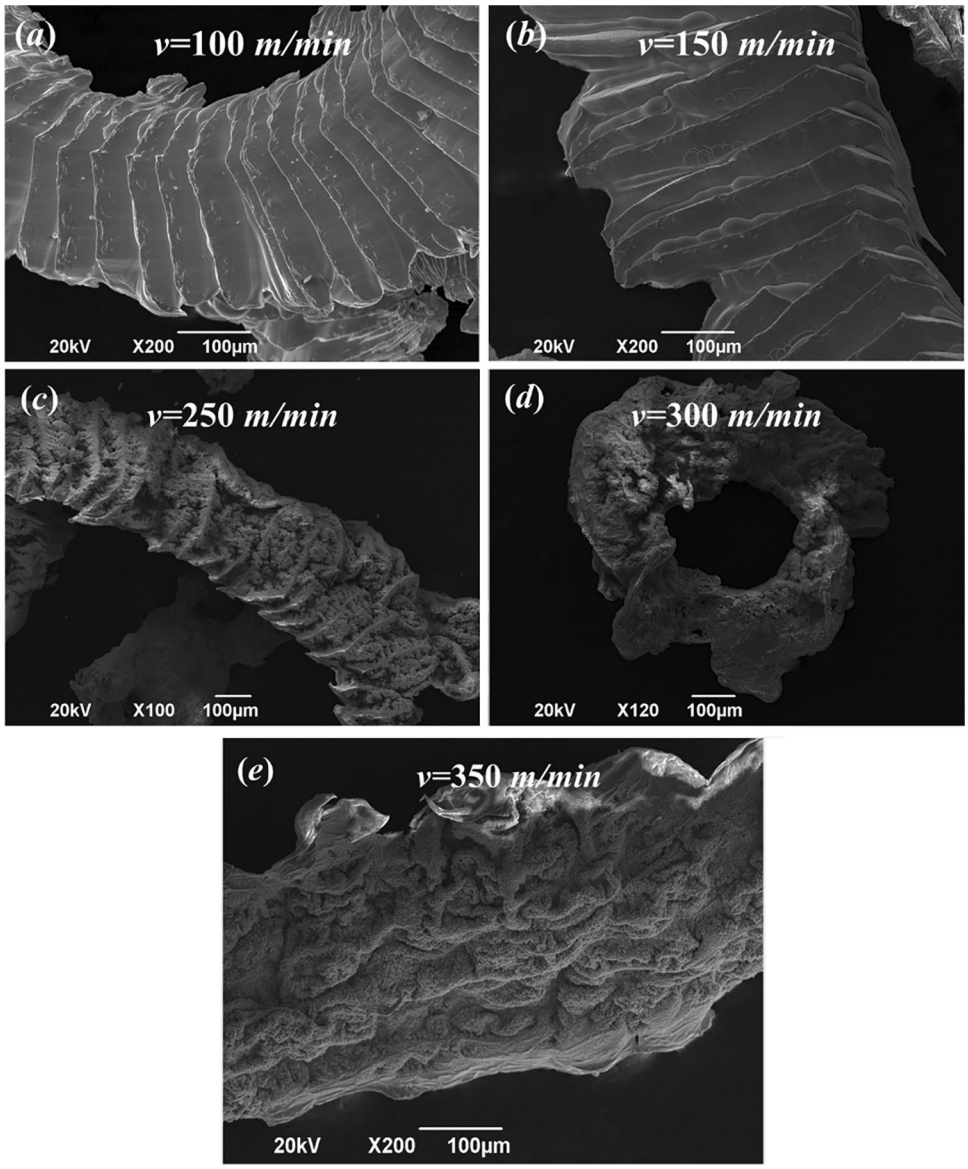

Fig. 8 SEM micrographs of the Zr57 BMG chips at different cutting speeds

by powder particles. Therefore, the temperature rise could be the main reason for the variation of chip morphology, especially at high cutting speeds. The powder particles were the products of chip surface oxidation, and the degree of chip surface oxidation increased with the increase of cutting speed.

Differing from Zr57 BMG, Zr702 is a traditional crystalline metal material, which has better plasticity and higher thermal conductivity. The SEM micrographs of Zr702 chips are presented in Fig. 9a–c. Serrated chips were also observed for Zr702, while the serrations were not obvious when compared with Zr57 BMG, which may be due to the better plasticity of Zr702. Moreover, no molten droplet was found on the chips because the thermal conductivity and melting point of Zr702 are higher than those of Zr57 BMG. Generally, Zr702 has higher thermal conductivity and the rise of temperature could be smaller than that of Zr57 BMG.

3.4 Tool wear

In order to study the tool wear during the high-speed machining of Zr57 BMG, the machining tests were conducted at three cutting speeds of 150, 200, and 350 m/min, respectively. Six Zr57 BMG rod specimens were machined for each tool by use of the fixture device as shown in Fig. 1. During machining, the cutting depth and feed rate were kept constant as 0.2 mm and 0.08 mm/r, respectively. The SEM micrographs of the flank faces of the worn tools were given in Fig. 10. A large amount of adhensions were found on the tool flank faces. It indicated that both the abrasive wear and adhesive wear were responsible for the

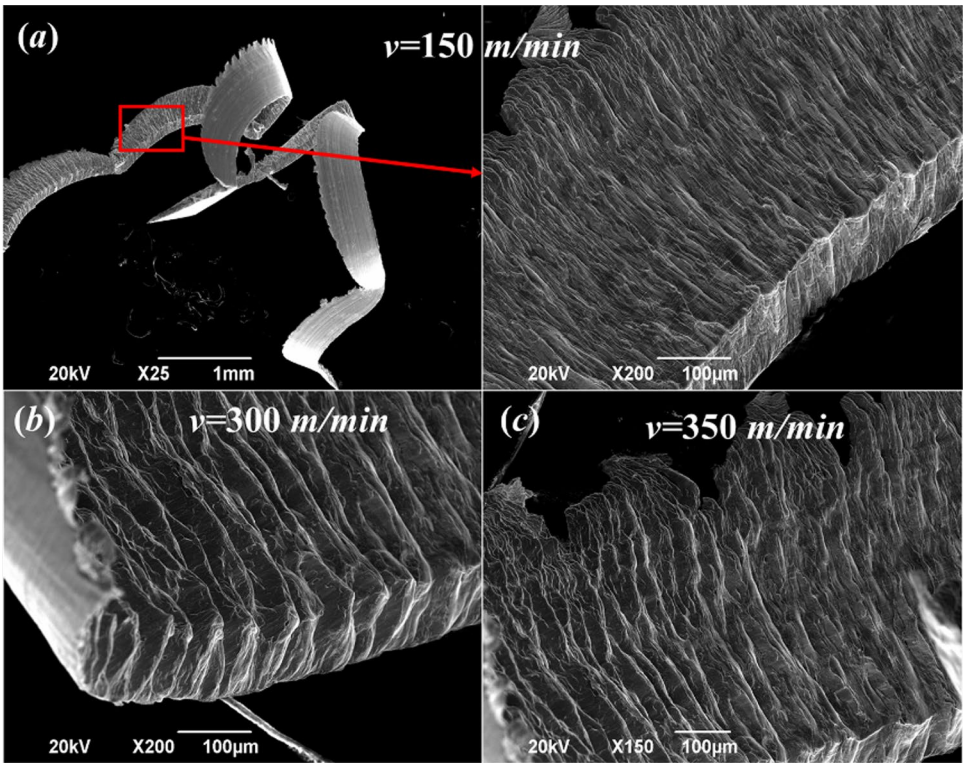

Fig. 9 SEM micrographs of the Zr702 chips at different cutting speeds

main wear behavior of tools during the high-speed machining of Zr57 BMG. The abrasive wear was mainly caused by the high hardness of the material, and the adhesive wear was mainly due to the high cutting temperature and low melting point of the material. Additionally, the degree of tool wear can be expressed by the maximum wear parameter (VB_{max}) on the flank face. As shown in Fig. 10, the VB_{max} increased from 69.5 to 126.9 μm with the increasing of cutting speed. Therefore, the wear behavior will also be serious when the cutting speed increases to 350 m/min.

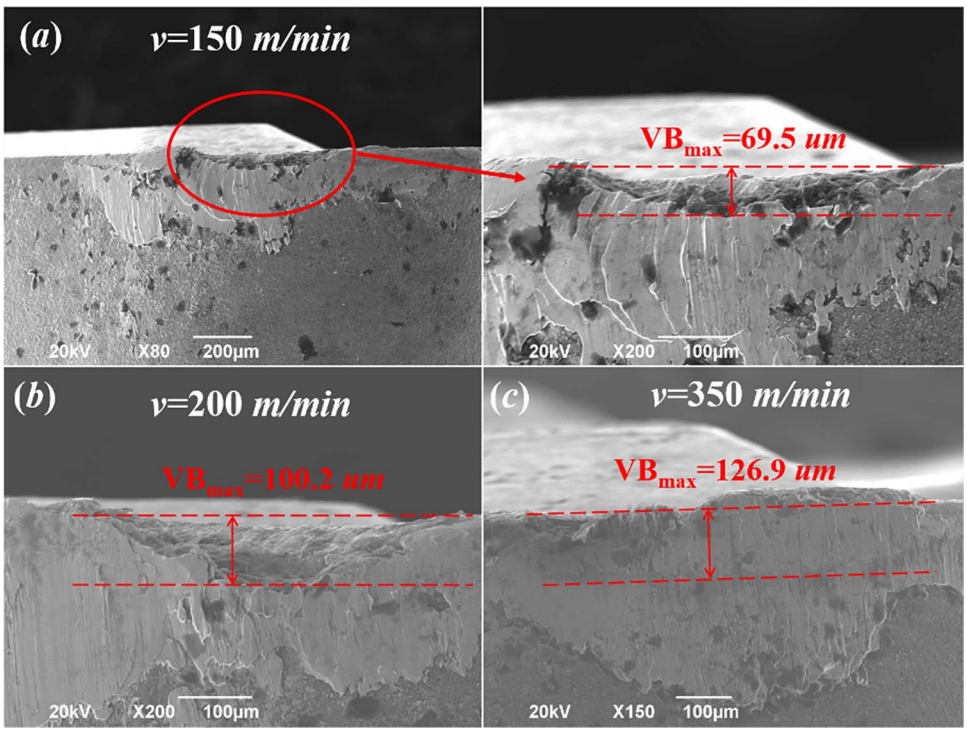

Fig. 10 SEM micrographs of the flank faces of worn tools at different cutting speeds

3.5 Cutting parameters optimization

Surface quality plays an important role during the machining of mechanical parts, which is influenced by the cutting parameters, such as cutting speed, feed rate, and cutting depth. Besides the effect of cutting speed on the cutting characteristics during the high-speed machining of BMGs, orthogonal experiment was further designed and conducted based on abovementioned results, in order to further study the effect of cutting depth and feed rate on surface roughness. The cutting parameters were further optimized based on the obtained surface roughness data. During the orthogonal tests, each cutting parameter had five levels. The cutting speed increased from 250 to 350 m/min, the feed rate increased from 0.039 to 0.12 mm/r, and the cutting depth increased from 0.05 to 0.25 mm. The range of cutting speed was selected because the distribution of wave patterns on the machined surfaces became regular and the surface quality was also improved within this range. The cutting parameters as well as the surface roughness data of the orthogonal experiments were shown in Table 3. As compared with the surface roughness data as shown in Fig. 3, the optimized results show much smaller surface roughness reaching 0.72 μm.

Based on the orthogonal experimental results, the influence of each cutting parameter on surface roughness was shown in Fig. 11. It can be seen that variation trends of the surface roughness data on the change of cutting speed, feed rate, and cutting depth were almost the same. Especially, the surface roughness increased initially and then decreased with the increase of cutting speed, which was different from the results in Sect. 3.2 where the cutting depth and feed rate were kept as constant. Here, low cutting depth and low feed rate were used, resulting in relatively lower cutting temperature. Combined with the influence of surface morphology on surface roughness, the appearance of irregular wave patterns and regular distribution of wave patterns should correspond to the increase and decrease of surface roughness in Fig. 11. It also indicated that in order to achieve better surface quality, the use of high cutting speed, low feed rate, and low cutting depth were beneficial to improve the surface roughness. For the present work, a better surface roughness can be obtained at the speed of 350 m/min, feed rate of 0.039 mm/r, and cutting depth of 0.05 mm.

As a new kind of metallic materials, BMGs have unique mechanical and physical properties and wide range of application prospects [24–27]. Although the Zr57 BMG has a high strength of about 1.64 GPa, the main cutting force is relatively small, as compared with the conventional Zr702.

Table 3 Cutting parameters as well as the surface roughness data for orthogonal experiment

No	Cutting speed (m/min)	Feed rate (mm/r)	Cutting depth (mm)	Ra (μm)
1	250	0.039	0.05	0.720
2	250	0.054	0.15	2.140
3	250	0.08	0.25	2.540
4	250	0.1	0.1	2.247
5	250	0.12	0.2	1.755
6	275	0.039	0.25	1.787
7	275	0.054	0.1	2.284
8	275	0.08	0.2	2.845
9	275	0.1	0.05	2.595
10	275	0.12	0.15	1.679
11	300	0.039	0.2	2.261
12	300	0.054	0.05	1.829
13	300	0.08	0.15	2.494
14	300	0.1	0.25	1.971
15	300	0.12	0.1	2.601
16	325	0.039	0.15	2.235
17	325	0.054	0.25	1.746
18	325	0.08	0.1	1.952
19	325	0.1	0.2	1.904
20	325	0.12	0.05	1.948
21	350	0.039	0.1	1.104
22	350	0.054	0.2	1.387
23	350	0.08	0.05	1.390
24	350	0.1	0.15	2.079
25	350	0.12	0.25	1.894

The surface morphology of Zr57 BMG is obviously influenced by the temperature during machining, where groove marks and adhensions were formed initially and then evolved to wave patterns and molten droplets. The appearance of wave patterns tends to reduce the surface quality. Although a large amount of heat will be generated during high-speed cutting, the machined surfaces of Zr57 BMG specimen still maintain the pure amorphous atomic structures during high-speed machining (100–350 m/min). Both abrasive wear and adhesive wear play significantly roles during the high-speed machining of Zr57 BMG. The use of high cutting speed, low feed rate, and cutting depth is beneficial for improving the surface roughness. The present findings have shown that high-speed machining can be used to process BMG and BMG components for widespread engineering applications [24]. Moreover, the high-speed machining can also be used to improve the machining efficiency and surface quality of BMGs by not altering the material properties.

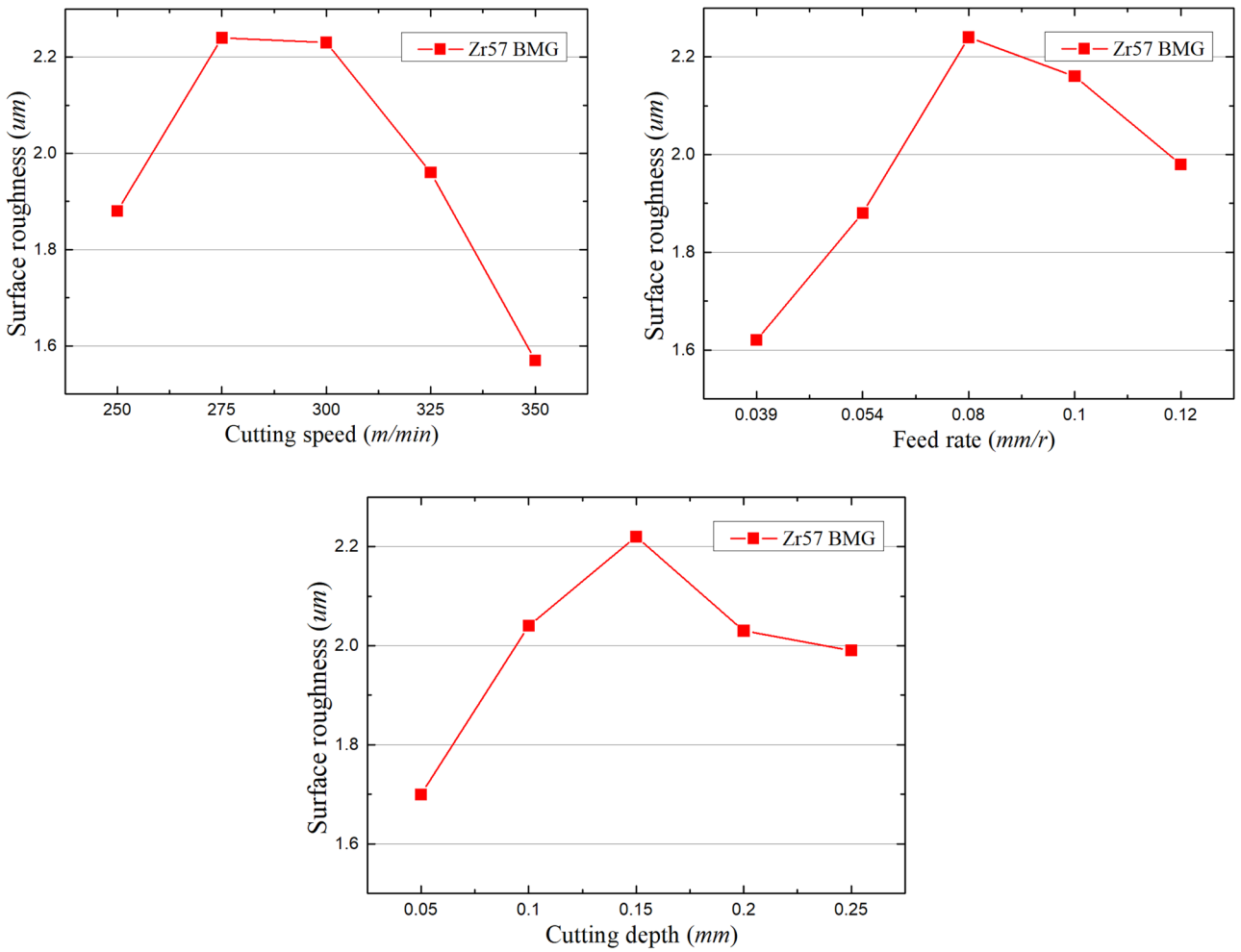

Fig. 11 Influence of each cutting parameter on surface roughness

4 Conclusions

High-speed machining Zr57 BMG was carried out in this work. The effect of cutting speed on cutting force, surface roughness, surface morphology, chip morphology, and tool wear was investigated and discussed, and the conclusions were summarized as follows:

(1) The extremely high yield strength and hardness of Zr57 BMG could be the main reason for the high radial force. However, although the strength of Zr57 BMG is much higher than that of conventional Zr702, the difference in main cutting force was small, which could be mainly attributed to the thermal softening of Zr57 BMG material during machining.

(2) For Zr57 BMG, with the cutting speed increasing from 100 to 350 m/min, the machined surface morphology of groove marks and adhensions evolved to wave patterns and molten droplets. The reduction of adhensions was beneficial for improving the surface quality, while the appearance of irregular wave patterns tends to destroy the surface quality. When the distribution of wave patterns becomes regular, the surface quality will also be improved. The machined surfaces of Zr57 BMG still maintain the amorphous atomic structures after high-speed machining (100–350 m/min).

(3) During the high-speed machining of Zr57 BMG, the free surface morphology of the chips, with cutting speed smaller than 150 m/min, showed obvious serration and molten droplets between shear bands. Differing from Zr702, oxidation occurred on the chip surfaces, which was gradually covered by powder particles when the cutting speed increased from 250 m/min to 350 m/min.

(4) Abrasive wear and adhesive wear were the main wear behavior on the tool flank face during the high-speed machining of Zr57 BMG. Further optimizations, based on orthogonal experimental at relatively high cutting

speed (from 250 to 350 m/min), have shown that the surface quality of the machined surface can be further improved by use of cutting parameters with high cutting speed, low feed rate and low cutting depth.

Author contribution Haidong Yang: Conceptualization, methodology, validation, writing original draft. Yusong Wu: Methodology, writing original draft. Junsheng Zhang: Review, conceptualization, methodology, validation, writing-review and editing. Huohong Tang: Formal analysis, writing-review and editing. Weijie Chang: Formal analysis, writing-review and editing. Juchen Zhang: Formal analysis, writing-review and editing. Shunhua Chen: Review, conceptualization, methodology, validation, writing-review and editing.

Funding This work was mainly supported by the Natural Science Foundation of Anhui Province (grant number 2108085ME171), Fundamental Research Funds for the Central Universities (grant number JZ2020HGTA0084), Key Laboratory of Electric Drive and Control of Anhui Higher Education Institutes, Anhui Polytechnic University (grant number DQKJ202101), and National Natural Science Foundation of China (grant number 51801049).

Availability of data and material The raw/processed data will be made available on request.

Code availability Not applicable.

Declarations

Ethics approval Not applicable.

Consent to participate Not applicable.

Consent for publication Not applicable.

Conflict of interest The authors declare no competing interests.

References

1. Schroers J (2010) Processing of bulk metallic glass. Adv Mater 22(14):1566–1597
2. Xia XQ, Zhang JS, Zou YM (2016) An investigation on the machinability of newly developed low-carbon sulphurised free-cutting steels. P I Mech Eng B-J Eng 230(9):1592–1599
3. Ma LJ, Sun ZC, Zhang L, Deng H, Tan YQ, Kong Z, Wei ZQ (2020) Study on mechanism and theoretical model of tool wear in fluorophlogopite glass-ceramics turning. J Mater Process Tech 275:116284
4. Ding F, Wang CY, Zhang T, Zheng LJ, Zhu XG, Li WR, Li LG (2020) Investigation on chip deformation behaviors of Zr-based bulk metallic glass during machining. J Mater Process Tech 276:116404
5. Chen SH, Ge Q, Zhang JS, Chang WJ, Zhang JC, Tang HH, Yang HD (2021) Low-speed machining of a Zr-based bulk metallic glass. J Manuf Process 72:565–581
6. Wang WH, Dong C, Shek CH (2004) Bulk metallic glasses. Mater Sci Eng R 44(2–3):45–89
7. Bakkal M, Shih AJ, Scattergood RO (2004) Chip formation, cutting forces, and tool wear in turning of Zr-based bulk metallic glass. Int J Mach Tools Manuf 44(9):915–925
8. Bakkal M, Shih AJ, Samuel BM, Liu CT, Scattergood RO (2005) Light emission, chip morphology, and burr formation in drilling the bulk metallic glass. Int J Mach Tools Manuf 45(7–8):741–752
9. Bakkal M, Nakşler V (2009) Cutting mechanics of bulk metallic glass materials on meso-end milling. Mater Manuf Process 24(12):1249–1255
10. Bakkal M, Serbest E, Karipçin İ, Kuzu AT, Karagüzel U, Derin B (2015) An experimental study on grinding of Zr-based bulk metallic glass. Adv Manuf 3(4):282–291
11. Fujita K, Morishita Y, Nishiyama N, Kimura H, Inoue A (2005) Cutting characteristics of bulk metallic glass. Mater Trans 46(12):2856–2863
12. Bakkal M, Liu CT, Watkins TR, Scattergood RO, Shih AJ (2004) Oxidation and crystallization of Zr-based bulk metallic glass due to machining. Intermetallics 12(2):195–204
13. Zhang WG, Ma MZ, Song AJ, Liang SX, Hao QH, Tan CL, Liu JR (2011) Temperature rise and flow of Zr-based bulk metallic glasses under high shearing stress. Sci China Phys Mech 54(11):1972–1976
14. Gong YD, Liu Y, Sun Y, Wen XL, Li Q, Qu SS, Cai M (2018) Experimental and emulational investigations into grinding characteristics of Zr-based bulk metallic glass (BMG) using microgrinding. Int J Adv Manuf Technol 97(9–12):3431–3451
15. Chen X, Xiao JF, Zhu Y, Tian RJ, Shu XW, Xu JF (2017) Micromachinability of bulk metallic glass in ultra-precision cutting. Mater Design 136:1–12
16. Zhu PZ, Qiu C, Fang FZ, Yuan DD, Shen XC (2014) Molecular dynamics simulations of nanometric cutting mechanisms of amorphous alloy. Appl Surf Sci 317:432–442
17. Wang M, Xu BS, Dong SY, Zhang JY, Wei SC (2013) Experimental investigations of cutting parameters influence on cutting forces in turning of Fe-based amorphous overlay for remanufacture. Int J Adv Manuf Technol 65(5–8):735–743
18. Bakkal M (2012) Machinability of BMG Key Eng Mater 521:225–253
19. Ye GG, Xue SF, Tong XH, Dai LH (2012) Slip-line field modeling of orthogonal machining pressure sensitive materials. Int J Adv Manuf Technol 58(9–12):907–914
20. Jiang MQ, Dai LH (2009) Formation mechanism of lamellar chips during machining of bulk metallic glass. Acta Mater 57(9):2730–2738
21. Maroju NK, Jin XL (2019) Mechanism of chip segmentation in orthogonal cutting of Zr-based bulk metallic glass. J Manuf Sci E-T ASME 141(8):081003–081013
22. Dhale K, Banerjee N, Singh RK, Outeiro JC (2019) Investigation on chip formation and surface morphology in orthogonal machining of Zr-based bulk metallic glass. Manuf Let 19:25–28
23. Chen SH, Chan KC, Xia L (2015) Fracture morphologies of Zr-based bulk metallic glasses under different stress states. Adv Eng Mater 17(3):366–373
24. Chen SH, Cheng HY, Chan KC, Wang G (2018) Metallic glass structures for mechanical-energy-dissipation purpose: a review. Metals 8:689
25. Chen SH, Yue TM, Tsui CP, Chan KC (2016) Flaw-induced plastic-flow dynamics in bulk metallic glasses under tension. Sci Rep 6:36130
26. Chen SH, Li T, Chang WJ, Yang HD, Zhang JC, Tang HH, Feng SD, Wu FF, Wu YC (2020) On the formation of shear bands in a metallic glass under tailored complex stress fields. J Mater Sci Technol 18:112–117
27. Li HF, Zheng YF (2016) Recent advances in bulk metallic glasses for biomedical applications. Acta Biomater 36:1–20